JACS
JOURNAL OF THE AMERICAN CHEMICAL SOCIETY
Article
Cite This: J. Am. Chem. Soc. 2018, 140, 14740−14746
pubs.acs.org/JACS

Single-Crystal Electrochemistry Reveals Why Metal Nanowires Grow

Myung Jun Kim,[†] Samuel Alvarez,[†] Zihao Chen,[‡] Kristen A. Fichthorn,[‡] and Benjamin J. Wiley*[,†]

[†]Department of Chemistry, Duke University, 124 Science Drive, Box 90354, Durham, North Carolina 27708, United States
[‡]Department of Chemical Engineering, The Pennsylvania State University, University Park, Pennsylvania 16802, United States

Supporting Information

ABSTRACT: Shape-control is used to tune the properties of metal nanostructures in applications ranging from catalysts to touch screens, but the origins of anisotropic growth of metal nanocrystals in solution are unknown. We show single-crystal electrochemistry can test hypotheses for why nanostructures form and predict conditions for anisotropic growth by quantifying the degree to which different species cause facet-selective metal deposition. Electrochemical measurements show disruption of alkylamine monolayers by chloride ions causes facet-selective Cu deposition. An intermediate range of chloride concentrations maximizes facet-selective Cu deposition on single crystals and produces the highest aspect ratio nanowires in a solution-phase synthesis. DFT calculations similarly show an intermediate monolayer coverage of chloride displaces the alkylamine capping agent from the ends but not the sides of a nanowire, facilitating anisotropic growth.

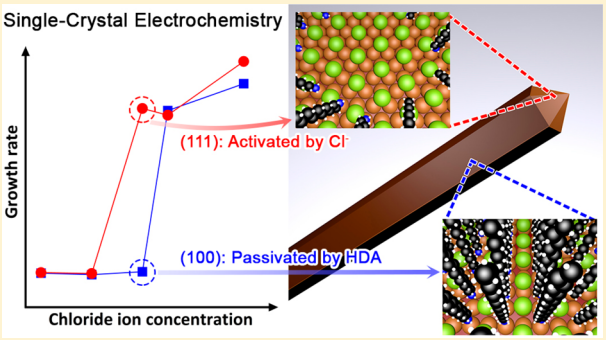

INTRODUCTION

Metal nanowires are essentially sticks of metal with diameters usually in the tens of nanometers and lengths in the tens of micrometers, giving them aspect ratios around 100−1000. The large aspect ratio of nanowires sets them apart from other nanostructures and allows them to form interconnected networks at low area coverages on surfaces and low volume fractions in bulk composites. Transparent, conductive films made from interconnected networks of nanowires are used in touch screens, with commercialization efforts underway for applications in organic light-emitting diodes and photovoltaics.[1−5] Metal nanowires have also been used in flexible/stretchable conductors,[6] wearable electronics,[7] biomedical devices,[8] electrocatalytic systems,[9−12] and lithium ion batteries.[13−15] Although metal nanowires can be produced with chemical vapor deposition[16] and electrochemical deposition in templates,[17] solution-phase synthesis can produce the largest amounts of nanowires at the lowest cost and, thus, is the principal means by which metal nanowires are produced for commercial applications.[18−20] Solution-phase synthesis generally involves heating a solution containing a metal salt, a reducing agent, and a shape-directing additive (usually referred to as a capping agent) that is necessary for anisotropic growth. Since the nanowire shape does not minimize surface energy, they are sometimes referred to as kinetically controlled shapes to reflect the fact that the shape is the result of a difference in the rate of atomic addition to different crystal facets.[18] For pentagonally twinned nanowires of Cu, Ag, and Au with {100} facets on their sides and {111} facets on their ends, researchers have hypothesized that organic capping agents direct anisotropic growth by selectively inhibiting atomic addition to the {100} facets.[18−20]

However, there is little experimental evidence to support the hypothesis that capping agents bind onto {100} facets and prevent metal deposition with a high selectivity. In addition, this hypothesis does not explain why most syntheses require the presence of halide ions to grow Cu, Ag, and Au nanowires (Table S1) or why the type of halide present in solution can affect nanostructure shape. For example, Au nanorods grow in the presence of cetyltrimethylammonium bromide (CTAB), but addition of iodide to the same synthesis results in the formation of nanoprisms.[21] Several hypotheses have been proposed to explain the role of halides and capping agents in this and other syntheses,[22] but it has proven difficult to eliminate some of these hypotheses through studies that take images of dried or frozen nanostructures at different stages of a synthesis. Although *in situ* visualization can help to distinguish between different growth mechanisms (e.g., atomic addition versus oriented attachment), such methods have not provided much insight into the facet-selective chemistry that drives anisotropic growth.[23,24] Most direct tests of hypotheses for why anisotropic growth occurs have been performed with computer simulations,[25−29] but more experimental evidence is necessary to corroborate these calculated results and determine which theories are most likely to be correct.[30]

Electrochemical measurements with single crystals can be used to better understand the facet-selective chemistry that drives anisotropic growth of metal nanowires, but there are

Received: July 29, 2018
Published: October 12, 2018

DOI: 10.1021/jacs.8b08053
J. Am. Chem. Soc. 2018, 140, 14740−14746

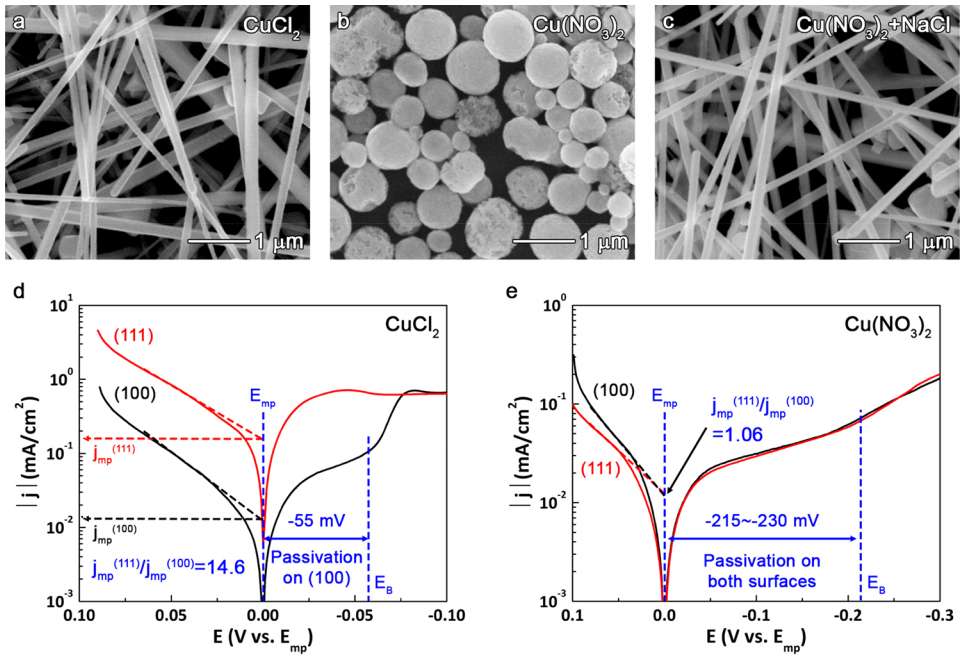

Figure 1. Cu nanostructures synthesized from (a) $CuCl_2$, (b) $Cu(NO_3)_2$, and (c) $Cu(NO_3)_2$ with NaCl in the presence of HDA and ascorbic acid. Tafel plots for the electrolytes containing (d) $CuCl_2$ and (e) $Cu(NO_3)_2$ with HDA and ascorbic acid.

very few such studies. For example, Burgess et al. studied the adsorption of a quaternary ammonium surfactant and bromide ions on Au(100) and Au(111), but they found no evidence of facet-selective adsorption.[31] In another electrochemical study with Cu(100) and Cu(111), Kim et al. showed that, rather than acting as a capping agent, ethylenediamine acts as a facet-selective promoter of Cu nanowire growth by keeping the Cu(111) surface relatively free of surface oxidation in the highly basic growth solution (>12 M NaOH).[32] These two studies with single crystals have already begun to challenge existing hypotheses for the role of capping agents in nanowire growth, but to date single-crystal electrochemical measurements have been performed with relatively few capping agents, they have not provided facet-dependent rates of atomic addition, and they have not yet revealed the role of halides in driving anisotropic growth of nanowires.

There is another synthesis of Cu nanowires that involves the reduction of $CuCl_2$ in the presence of alkylamines.[20,33] Liu et al. used density functional theory (DFT) to show hexadecylamine (HDA) forms self-assembled monolayers that bind Cu(100) slightly more strongly (by 0.12 eV) than Cu(111), but it is unclear whether this small difference in energy is sufficient to drive anisotropic growth.[28] In addition, the calculated binding energy of HDA to both Cu surfaces is ~60 times kT, meaning that the probability for spontaneous desorption of HDA is vanishingly small. It is unclear how Cu nanowires can grow if strongly adsorbed HDA passivates Cu surfaces and prevents electrochemical reactions from occurring, as has been observed experimentally.[33] Until now, there is no direct experimental evidence to clearly address these questions and better connect results from experimental syntheses to those from computer simulations.

This article provides evidence for a new mechanism by which both a capping agent, HDA, and Cl^- synergistically promote anisotropic growth of Cu nanowires. Electrochemical measurements on Cu(111) and Cu(100) surfaces show that, in contrast to previous hypotheses, HDA does not selectively passivate Cu(100); it passivates both facets equally. However, the introduction of Cl^- in a narrow range of concentrations selectively disrupts the alkylamine monolayer on Cu(111), causing Cu to preferentially deposit onto {111} facets on the ends of the nanowires. DFT calculations show that HDA and Cl chemically adsorb to both Cu(111) and Cu(100) at sufficiently low Cl coverages and that HDA physically adsorbs at high Cl coverages. As in experiments, DFT calculations indicate there is a narrow, intermediate Cl coverage window, where HDA chemisorbs to Cu(100), but physisorbs to Cu(111). Thus, anisotropic growth occurs via Cu atom addition to the less-protected {111} facets on nanowire ends.

RESULTS AND DISCUSSION

Roles of Cl^- and Hexadecylamine in Cu Nanowire Growth. Figure 1a shows that reduction of Cu ions in an aqueous solution of HDA and ascorbic acid leads to the formation of Cu nanowires with $CuCl_2$ as the Cu source. However, only spherical particles that are a mixture of metallic Cu and Cu_2O form if $Cu(NO_3)_2$ is used (Figures 1b and S1). Adding NaCl to the reaction with $Cu(NO_3)_2$ recovers the nanowire shape (Figure 1c). The same phenomena were observed using glucose as a reducing agent (Figure S2), indicating it does not depend on the electron source for Cu reduction. These results indicate that the presence of Cl^- is necessary for anisotropic growth and suggest that selective adsorption of HDA to {100} facets cannot by itself cause anisotropic growth of Cu nanowires.

Metal nanostructures grow through two simultaneous electrochemical reactions, oxidation of a reducing agent and reduction of a metal ion complex. These reactions must take place at the same rate to prevent the accumulation of charge. The potential at which the currents from the two redox reactions are equal is called the mixed potential (E_{mp}). E_{mp} can be determined electrochemically by sweeping the potential at an electrode immersed in the reaction solution and measuring the potential at which the current is zero (Figure S3). We used

DOI: 10.1021/jacs.8b08053
J. Am. Chem. Soc. 2018, 140, 14740−14746

E_{mp} as the reference potential since it is nearly the same for both surfaces. Figure 1d shows the current from Cu(111) is much larger than the current from Cu(100) in the nanowire reaction solution. The current at very positive potentials (left-hand side of the plot) is mostly from oxidation of ascorbic acid (the reducing agent), and the current at very negative potentials is mostly from the reduction of a Cu^+−HDA complex (Figure S4). The current from oxidation of ascorbic acid and reduction of the Cu^+−HDA complex is equal at E_{mp}, resulting in a net current of zero.

For a kinetically limited process, one can determine the current from either half-reaction by finding the intercept of the linear Tafel lines at E_{mp} (see Supporting Information for a detailed explanation). This was done for the current from ascorbic acid oxidation in Figure 1d because the current for the Cu^+−HDA complex reduction was mass transport-limited at potentials negative of −0.025 V (vs E_{mp}). Using this methodology, we found the current densities at E_{mp} for the Cu(111) and Cu(100) surfaces were $j_{mp}^{(111)}$ = 185 μA/cm^2 and $j_{mp}^{(100)}$ = 12.6 μA/cm^2, respectively. This means that reduction of the Cu^+−HDA complex was 14.7 times faster on Cu(111) than on Cu(100) in the presence of Cl^-. In other words, the charge-transfer resistance for the electrochemical reactions on Cu(111) was 14.7 times lower than on Cu(100). Figure 1e shows that, in the absence of Cl^-, there is no difference in the voltammograms for Cu(111) and Cu(100), and $j_{mp}^{(111)}/j_{mp}^{(100)}$ = 1.06 ($j_{mp}^{(111)}$ = 11.71 μA/cm^2 and $j_{mp}^{(100)}$ = 11.09 μA/cm^2), indicating HDA alone does not act as a facet-selective capping agent. The presence of HDA does, however, greatly reduce the current at the mixed potential. Figure S5 shows linear sweep voltammograms and the corresponding Tafel plots for solutions containing only $Cu(NO_3)_2$ and ascorbic acid, demonstrating that the value of the j_{mp} is higher in the absence of HDA (j_{mp}: 322 μA/cm^2 for Cu(111) and 356 μA/cm^2 for Cu(100), but does not exhibit facet-selectivity.

To compare the stability of the alkylamine monolayer in the presence and absence of Cl^-, one can use the breakdown potential (E_B). E_B is the potential at which there is an abrupt increase in the slope of the I−V curve (Figure S3), which indicates the breakdown of the HDA passivation layer. Without Cl^-, this breakdown occurs at 215−230 mV (vs E_{mp}) for both Cu(111) and Cu(100). Upon addition of Cl^-, breakdown occurs at ∼55 mV for Cu(100) and removes any passivation effect for Cu(111), indicating the presence of Cl^- decreases the stability of the alkylamine monolayer. In addition, at this Cl^- concentration, HDA can still passivate Cu(100) but provides no passivation for Cu(111). These results led us to hypothesize that the anisotropic growth of Cu nanowires is enabled by a facet-selective disruption of the HDA monolayer by Cl^-.

Predicting Changes in Cu Nanowire Shape by Single-Crystal Electrochemistry. We next set out to test this hypothesis by studying whether there is a correlation between the effect of Cl^- on the electrochemistry occurring on bulk single crystals and nanowires. Figure 2 summarizes values of j_{mp} and E_B that were extracted from Tafel plots at different Cl^- concentrations (Figure S6). Figure 2a shows that, at both low and high Cl^- concentrations, there is no difference in the j_{mp} between Cu(111) and Cu(100). It is only at an intermediate Cl^- concentration (32.8 mM) that the current is much larger on Cu(111) than on Cu(100). Figure 2b shows that the concentration at which the difference in the j_{mp} was the greatest was the same as the concentration at which the

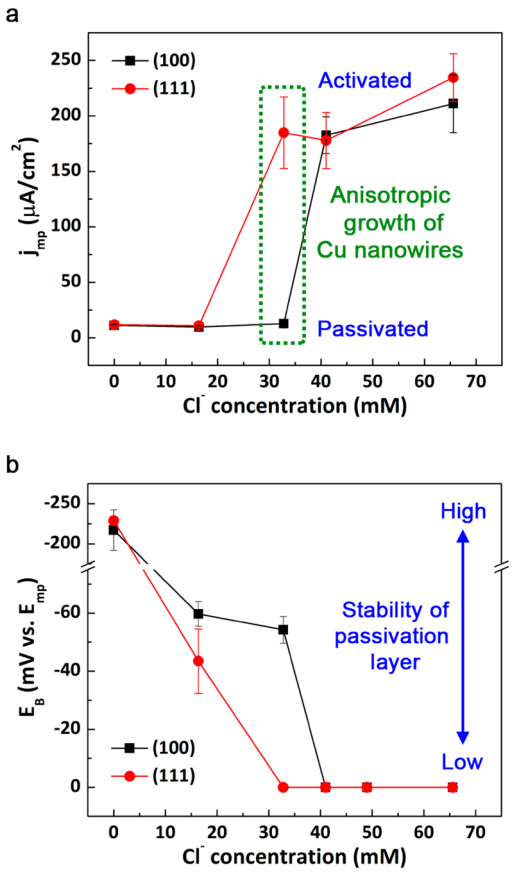

Figure 2. (a) Current density at E_{mp} and (b) breakdown potential for the HDA according to the Cl^- concentration for Cu(111) compared with Cu(100).

difference in the stability of the alkylamine monolayers was the greatest. Thus, Cl^- disrupts the alkylamine monolayer at both Cu(111) and Cu(100), but it does so on Cu(111) at a lower concentration of Cl^-. Furthermore, these single-crystal measurements enabled us to predict that the aspect ratio of Cu nanowires should depend on the concentration of Cl^-.

Images of Cu nanostructures synthesized with various concentrations of Cl^- are shown in Figure 3a−d (see also Figures S7 and S8). Figure 3e and f show how the average length and diameter of the Cu nanowires vary with the concentration of Cl^-. The longest and the thinnest Cu nanowires, i.e., those with the highest aspect ratio, were obtained with a Cl^- concentration of 32.8 mM. This is the same concentration that resulted in the largest ratio of $j_{mp}^{(111)}/j_{mp}^{(100)}$. At lower Cl^- concentrations (16.4 mM), the reaction mostly produced Cu nanoparticles with a few short nanowires. The large concentration of nanoparticles implies that there was not sufficient Cl^- to disrupt the HDA monolayer on the Cu{111} facets on the ends of nanowires and induce anisotropic growth. This result agrees with the fact that $j_{mp}^{(111)} \approx j_{mp}^{(100)}$ in the single-crystal electrochemical measurements at this concentration of Cl^-.

At relatively high concentrations of Cl^-, rather than forming nanoparticles, on average the diameter of the Cu nanowire increased, and the length decreased. Figure 3c and d show examples of the lateral growth that occurred as a result of atomic addition to the {100} facets on the sides of nanowires. At a Cl^- concentration of 65.6 mM, Cu nanowires exhibited a nonuniform diameter similar to the shape of a javelin. For

DOI: 10.1021/jacs.8b08053
J. Am. Chem. Soc. 2018, 140, 14740−14746

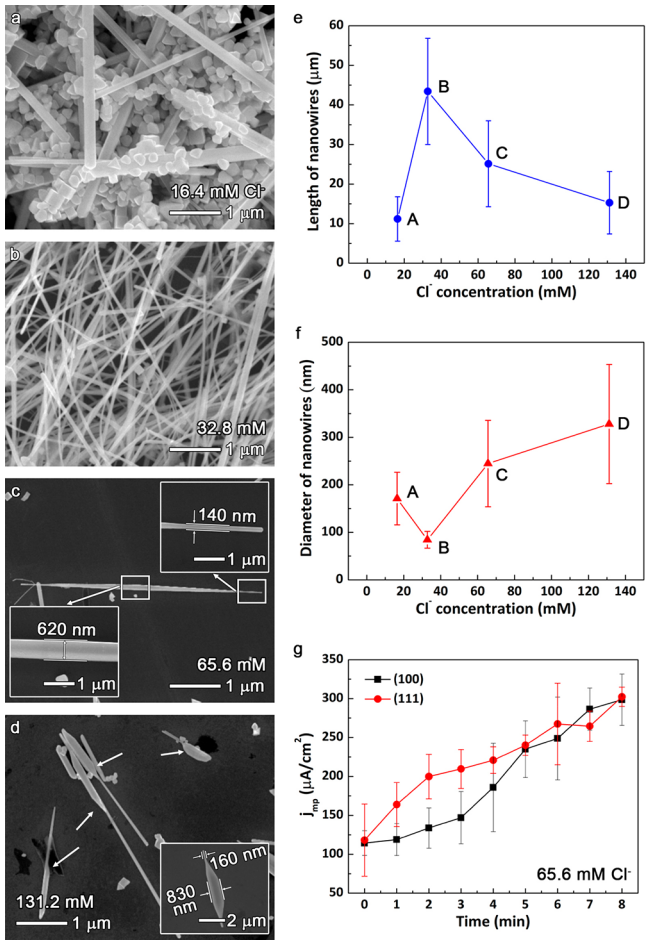

Figure 3. Cu nanostructures synthesized at Cl^- concentrations of (a) 16.4 mM, (b) 32.8 mM, (c) 65.6 mM, and (d) 131.2 mM. (e) Average length and (f) diameter of nanowires at different Cl^- concentrations. (g) Time-dependent change in j_{mp} for Cu(111) and Cu(100) single crystals at a Cl^- concentration of 65.6 mM.

example, the nanowire in Figure 3c has a diameter of 620 nm in the center and 140 nm at the ends. This suggests that growth along the longitudinal axis of the nanowire preceded growth of the diameter. The lateral growth of Cu nanowires was more prevalent with 131.2 mM Cl^- (white arrows in Figure 3d), indicating the higher concentration of Cl^- more effectively disrupted the HDA monolayer on {100} facets, resulting in increased atomic addition to the sides of the nanowires.

The shape of Cu nanostructures at high concentrations of Cl^- is indicative of a time-dependent disruption of the HDA monolayer. Thus, we returned to the single-crystal electrochemical experiments to determine if this time-dependent disruption could be observed in the changes in $j_{mp}^{(111)}$ and $j_{mp}^{(100)}$. The Tafel plots used for calculating $j_{mp}^{(111)}$ and $j_{mp}^{(100)}$ at various times are presented in Figure S9. Figure 3g shows that $j_{mp}^{(111)}$ increases faster than $j_{mp}^{(100)}$ in the first 4 min of the electrochemical measurements. Factors that could affect j_{mp} over time include changes in the structure of the alkylamine self-assembled monolayer, changes in the concentrations of the Cu precursor and reducing agent, and changes in the disruption of the self-assembled monolayer with Cl^-. In the absence of Cl^-, one would expect the HDA monolayer to be more defect-free and more passivating with time, leading to a decrease in the j_{mp}, but this is the opposite of what was observed experimentally. Decreases in the concentrations of the Cu precursor and reducing agent with time would also decrease j_{mp}, but this is again the opposite of what was observed experimentally. Therefore, we attribute the observed increase in j_{mp} to the time-dependent disruption of the HDA monolayer by Cl^-.

Given that nanowires grow at a rate of 4.2 μm/min with tetradecylamine as a capping agent,[33] and nanowires grow to similar lengths with HDA (suggesting a similar growth rate), these few minutes are sufficient for a nanowire to grow longitudinally before lateral growth ensues. Since Cu can be deposited on the electrodes as soon as the electrodes are immersed into the reaction solution, the electrochemical measurements for 8 min cover nearly the entire period of nanowire growth. This time-dependent growth explains why nanowires still formed at high concentrations of Cl^- that did not exhibit a facet-dependent j_{mp} at 5 min (Figure 2a). The greater stability of the HDA monolayer on Cu(100) results in it taking a longer time for the disruption to occur. Since nanowires in the alkylamine-mediated synthesis grow from both sides of a decahedral seed,[33] this time-dependent disruption leads to the formation of the javelin-shaped nanowire in Figure 3c.

Competitive Adsorption of Cl^- and HDA: DFT. To elucidate the roles of Cl^- and HDA in promoting anisotropic nanocrystal growth, we investigated their coadsorption on Cu(100) and Cu(111) using first-principles, dispersion-corrected DFT with the Vienna ab Initio Simulation Package (VASP).[34−36] We considered Cl coverages ranging from 0.0 to 0.5 monolayer (ML) and HDA self-assembled layers at coverages ranging from 0.25 to maximum coverages of 0.40 ML on Cu(100) and 0.33 ML on Cu(111) (Table S2).[28] We assume Cu surfaces are well-protected from solvent by HDA, such that water would reside above the self-assembled HDA monolayer and play a minor role in determining the structure and properties of the surface region. Thus, we do not include water in our calculations. Details of our calculations and convergence tests can be found in the Supporting Information.

In the absence of Cl, HDA forms passivating self-assembled monolayers on both surfaces.[28,29,33] The DFT surface energies for HDA-covered Cu(100) and Cu(111) are 0.087 and 0.079 eV/Å^2, respectively. With these surface energies, we predict that the Wulff shape of a Cu nanoparticle is a truncated octahedron,[37] which is consistent with the experimental observation of sphere-like particles in the absence of Cl^- (Figure 1b).

At a Cl coverage of 0.25 ML, HDA chemically adsorbs to both Cu surfaces (Figure 4a and b). The binding energy of HDA on 0.25 ML Cl−Cu(100) is higher than on bare Cu(100). We see that the Cu−N interaction nearly doubles from its bare-surface value (Table S3), which may be due to stronger ionic bonding that is reflected in higher charging of the N relative to the bare surface (Table S4). In contrast, HDA binding on Cu(111) is weakened compared to the bare surface at 0.25 ML Cl, likely due to repulsion from Cl atoms (Table S4), though the Cu−N interaction increases slightly (Table S3). The emergence of short nanowires among nanoparticles in the experiments (Figure 3a) coincides with this enhanced {100}-facet selectivity of HDA binding at low Cl coverages.

On increasing the Cl coverage to 0.33 ML, HDA moves away from Cu(111) (Figure 4d), likely due to the short-range repulsion that occurs as strongly bound Cl atoms "crowd out"

DOI: 10.1021/jacs.8b08053
J. Am. Chem. Soc. 2018, 140, 14740−14746

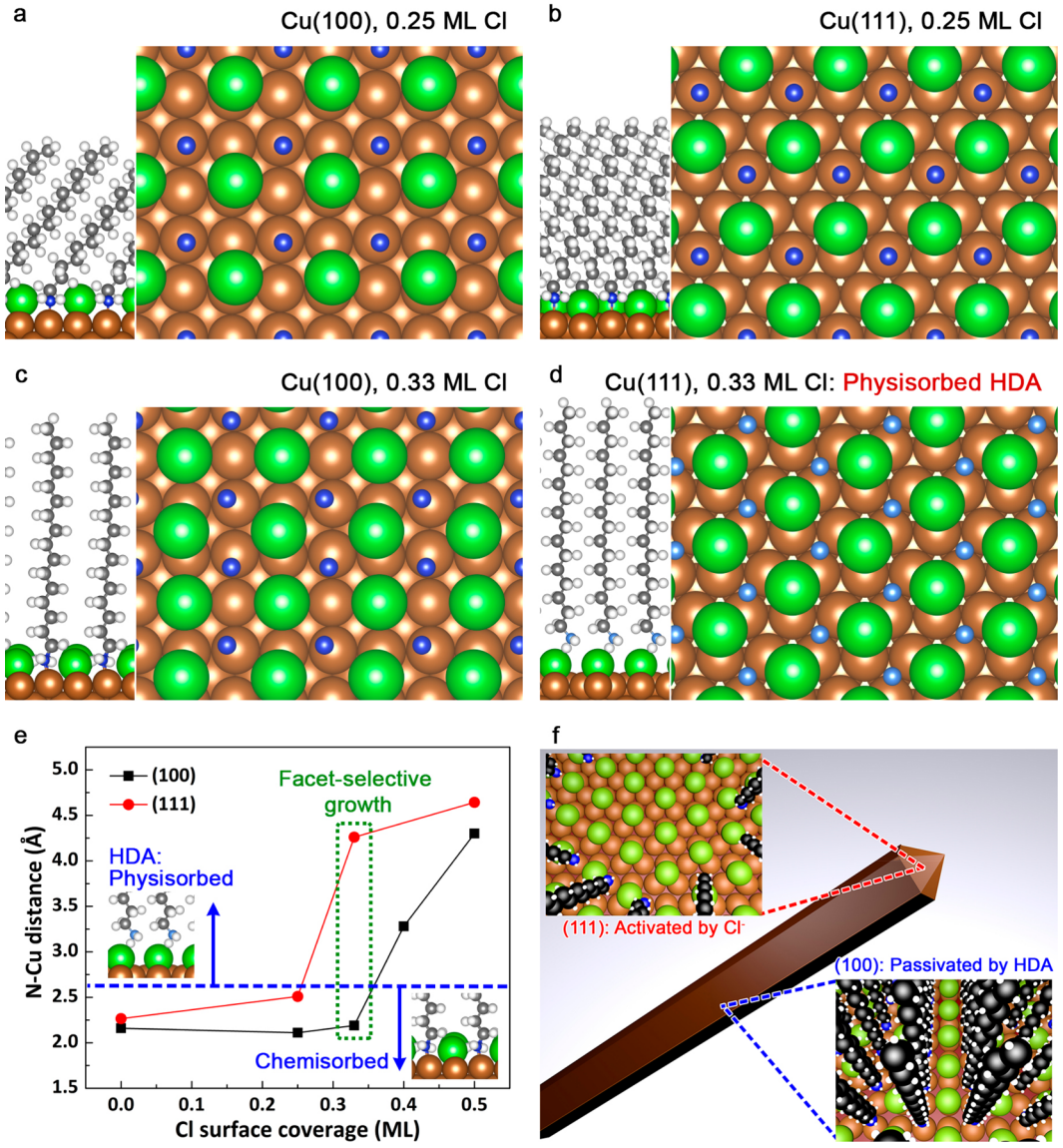

Figure 4. Top and side views for the optimized binding conformations of Cl and HDA at Cl coverages of (a) 0.25 ML on Cu(100), (b) 0.25 ML on Cu(111), (c) 0.33 ML on Cu(100), and (d) 0.33 ML on Cu(111) (brown: Cu, dark blue: chemisorbed N, light blue: physisorbed N, green: Cl). (e) Change in the distance between N and Cu according to Cl coverage. (f) Schematic diagram describing the mechanism for the anisotropic growth of Cu nanowires.

HDA, which has a weaker interaction with the Cu surface (Tables S3 and S5). As a result, HDA forms a physically adsorbed layer above the Cl surface layer, in which the interaction between the amine and the substrate is dominated by van der Waals attraction that is mitigated by electrostatic repulsion with the Cl layer (Tables S3 and S4). In contrast, Cu(100) can accommodate both Cl and HDA and is passivated with chemically bound HDA (Figure 4c). The weak physisorption of HDA on Cu(111) and the strong chemisorption of HDA on Cu(100) are consistent with electrochemical measurements (Figure 2) and nanowire formation (Figure 3b).

At a Cl coverage of 0.4 ML on Cu(100), we observe that disordered layers emerge (Figure S10), which consist of a mixture of physically and chemically adsorbed HDA molecules. We note that van der Waals attraction between the HDA alkyl tails promotes cohesion within these structures (Table S3). Finally, at a Cl coverage of 0.50 ML, the HDA adlayers become weakly physisorbed on both surfaces (Figures S11 and S15). The nonuniform javelin-like nanowires (Figure 3c and d), indicating a facilitated lateral growth, can be explained by reduced protection of both surfaces due to weakened HDA binding.

The average distance between N atoms in HDA and the top layer of Cu surface atoms is shown as a function of Cl coverage in Figure 4e. This graph closely resembles the trend of the j_{mp} as a function of the Cl^- concentration (Figure 2a). We note that the Cu−N bond strength exhibits similar behavior to the bond length (Figure S12). Only the intermediate coverage of 0.33 ML exhibits significant facet selectivity, such that HDA is weakly physisorbed on Cu(111) and chemisorbed on Cu(100), promoting the observed anisotropic growth.

A summary of the mechanism for anisotropic growth of Cu nanowires is illustrated in Figure 4f. The facet-dependent competitive adsorption of Cl^- and HDA promotes the anisotropic growth of Cu nanowires. At zero or low Cl

DOI: 10.1021/jacs.8b08053
J. Am. Chem. Soc. 2018, 140, 14740−14746

coverages on both surfaces, HDA molecules establish chemically adsorbed self-assembled monolayers that effectively passivate both surfaces and lead to spherical particles or short nanowires. As the Cl^- concentration (and Cl surface coverage) increases, we reach a surface coverage at which HDA has weak physical adsorption on Cu(111) and relatively strong chemical adsorption on Cu(100). The weakly bound HDA adlayer on Cu(111) leads to poor electrochemical passivation of the ends of nanowires compared to the {100} sides and the selective addition of Cu to the ends of nanowires. This scenario is confirmed by DFT calculations, synthetic results, and electrochemical results from Cu single crystals.

CONCLUSION

The synthesis and applications of metal nanostructures have advanced much more rapidly than the understanding of the mechanisms by which anisotropic growth occurs because of the lack of experimental methods that provide unambiguous tests of theoretical hypotheses. This article shows single-crystal electrochemistry is such a method, and we expect similar studies will clarify the facet-selective chemistry that drives anisotropic growth of Ag, Au, Pd, and Pt nanostructures. Such work will enable the development of nanostructure syntheses from a deeper understanding of facet-selective chemistry rather than from trial and error.

ASSOCIATED CONTENT

Supporting Information

The Supporting Information is available free of charge on the ACS Publications website at DOI: 10.1021/jacs.8b08053.

Materials and methods, supplementary text, figures, and tables (PDF)

AUTHOR INFORMATION

Corresponding Author

*benjamin.wiley@duke.edu

ORCID

Kristen A. Fichthorn: 0000-0002-4256-714X

Benjamin J. Wiley: 0000-0002-1314-6223

Notes

The authors declare no competing financial interest.

ACKNOWLEDGMENTS

We thank Y. Xia (Georgia Tech.), L. M. Liz-Marzán (CIC biomaGUNE), and T. P. Moffat (NIST) for helpful discussions. This work was supported by NSF Grant No. CHE-1808108 and DMR-1253534 (M.J.K., S.A., B.J.W.). This work was also supported by the Department of Energy, Office of Basic Energy Sciences, Materials Science Division, DE-FG02-07ER46414 (Z.C., K.A.F.). Z.C. also acknowledges training provided by the Computational Materials Education and Training (CoMET) NSF Research Traineeship (DGE-1449785).

REFERENCES

(1) Lee, J.-Y.; Connor, S. T.; Cui, Y.; Peumans, P. Solution-processed metal nanowire mesh transparent electrodes. *Nano Lett.* **2008**, *8*, 689−692.

(2) Ye, S.; Rathmell, A. R.; Chen, Z.; Stewart, I. E.; Wiley, B. J. Metal nanowire networks: the next generation of transparent conductors. *Adv. Mater.* **2014**, *26*, 6670−6687.

(3) Kang, S.; Kim, T.; Cho, S.; Lee, Y.; Choe, A.; Walker, B.; Ko, S. J.; Kim, J. Y.; Ko, H. Capillary printing of highly aligned silver nanowire transparent electrodes for high-performance optoelectronic devices. *Nano Lett.* **2015**, *15*, 7933−7942.

(4) Niu, Z.; Cui, F.; Yu, Y.; Becknell, N.; Sun, Y.; Khanarian, G.; Kim, D.; Dou, L.; Dehestani, A.; Schierle-Arndt, K.; Yang, P. Ultrathin epitaxial Cu@Au core−shell nanowires for stable transparent conductors. *J. Am. Chem. Soc.* **2017**, *139*, 7348−7354.

(5) Ahn, J.; Hwang, H.; Jeong, S.; Moon, J. Metal-nanowire-electrode-based perovskite solar cells: challenging issues and new opportunities. *Adv. Energy Mater.* **2017**, *7*, 1602751.

(6) Xu, F.; Zhu, Y. Highly conductive and stretchable silver nanowire conductors. *Adv. Mater.* **2012**, *24*, 5117−5122.

(7) Amjadi, M.; Pichitpajongkit, A.; Lee, S.; Ryu, S.; Park, I. Highly stretchable and sensitive strain sensor based on silver nanowire−elastomer nanocomposite. *ACS Nano* **2014**, *8*, 5154−5163.

(8) Park, J.; Choi, S.; Janardhan, A. H.; Lee, S.-Y.; Raut, S.; Soares, J.; Shin, K.; Yang, S.; Lee, C.; Kang, K.-W.; Cho, H. R.; Kim, S. J.; Seo, P.; Hyun, W.; Jung, S.; Lee, H.-J.; Lee, N.; Choi, S. H.; Sacks, M.; Lu, N.; Josephson, M. E.; Hyeon, T.; Kim, D.-H.; Hwang, H. J. Electromechanical cardioplasty using a wrapped elasto-conductive epicardial mesh. *Sci. Transl. Med.* **2016**, *8*, 344ra86.

(9) Koenigsmann, C.; Santulli, A. C.; Gong, K.; Vukmirovic, M. B.; Zhou, W. P.; Sutter, E.; Wong, S. S.; Adzic, R. R. Enhanced electrocatalytic performance of processed, ultrathin, supported Pd-Pt core-shell nanowire catalysts for the oxygen reduction reaction. *J. Am. Chem. Soc.* **2011**, *133*, 9783−9795.

(10) Li, H.-H.; Ma, S.-Y.; Fu, Q.-Q.; Liu, X.-J.; Wu, L.; Yu, S.-H. Scalable bromide-triggered synthesis of Pd@Pt core-shell ultrathin nanowires with enhanced electrocatalytic performance toward oxygen reduction reaction. *J. Am. Chem. Soc.* **2015**, *137*, 7862−7868.

(11) Fu, Q.-Q.; Li, H.-H.; Ma, S.-Y.; Hu, B.-C.; Yu, S.-H. A mixed-solvent route to unique PtAuCu ternary nanotubes templated from Cu nanowires as efficient dual electrocatalysts. *Sci. China Mater.* **2016**, *59*, 112−121.

(12) Li, H.-H.; Fu, Q.-Q.; Xu, L.; Ma, S.-Y.; Zheng, Y.-R.; Liu, X.-J.; Yu, S.-H. Highly crystalline PtCu nanotubes with three dimensional molecular accessible and restructured surface for efficient catalysis. *Energy Environ. Sci.* **2017**, *10*, 1751−1756.

(13) Lu, L.-L.; Ge, J.; Yang, J.-N.; Chen, S.-M.; Yao, H.-B.; Zhou, F.; Yu, S.-H. Free-standing copper nanowire network current collector for improving lithium anode performance. *Nano Lett.* **2016**, *16*, 4431−4437.

(14) Lu, L.-L.; Zhang, Y.; Pan, Z.; Yao, H.-B.; Zhou, F.; Yu, S.-H. Lithiophilic Cu−Ni core−shell nanowire network as a stable host for improving lithium anode performance. *Energy Storage Mater.* **2017**, *9*, 31−38.

(15) He, Z.; Yang, Y.; Liu, J.-W.; Yu, S.-H. Emerging tellurium nanostructures: controllable synthesis and their applications. *Chem. Soc. Rev.* **2017**, *46*, 2732−2753.

(16) Choi, H.; Park, S.-H. Seedless growth of free-standing copper nanowires by chemical vapor deposition. *J. Am. Chem. Soc.* **2004**, *126*, 6248−6249.

(17) Gao, T.; Meng, G.; Wang, Y.; Sun, S.; Zhang, L. Electrochemical synthesis of copper nanowires. *J. Phys.: Condens. Matter* **2002**, *14*, 355−363.

(18) Xia, Y.; Xiong, Y.; Lim, B.; Skrabalak, S. E. Shape-controlled synthesis of metal nanocrystals: simple chemistry meets complex physics? *Angew. Chem., Int. Ed.* **2009**, *48*, 60−103.

(19) Kim, F.; Sohn, K.; Wu, J.; Huang, J. Chemical synthesis of gold nanowires in acidic solutions. *J. Am. Chem. Soc.* **2008**, *130*, 14442−14443.

(20) Jin, M.; He, G.; Zhang, H.; Zeng, J.; Xie, Z.; Xia, Y. Shape-controlled synthesis of copper nanocrystals in an aqueous solution with glucose as a reducing agent and hexadecylamine as a capping agent. *Angew. Chem., Int. Ed.* **2011**, *50*, 10560−10564.

(21) Lohse, S. E.; Burrows, N. D.; Scarabelli, L.; Liz-Marzán, L. M.; Murphy, C. J. Anisotropic noble metal nanocrystal growth: the role of halides. *Chem. Mater.* **2014**, *26*, 34−43.

DOI: 10.1021/jacs.8b08053
J. Am. Chem. Soc. 2018, 140, 14740−14746

(22) Lohse, S. E.; Murphy, C. J. The quest for shape control: a history of gold nanorod synthesis. *Chem. Mater.* **2013**, *25*, 1250−1261.
(23) Liao, H.-G.; Cui, L.; Whitelam, S.; Zheng, H. Real-time imaging of Pt_3Fe nanorod growth in solution. *Science* **2012**, *336*, 1011−1014.
(24) Ye, S.; Chen, Z.; Ha, Y.-C.; Wiley, B. J. Real-time visualization of diffusion-controlled nanowire growth in solution. *Nano Lett.* **2014**, *14*, 4671−4676.
(25) Al-Saidi, W. A.; Feng, H.; Fichthorn, K. A. Adsorption of polyvinylpyrrolidone on Ag surfaces: insight into a structure-directing agent. *Nano Lett.* **2012**, *12*, 997−1001.
(26) Almora-Barrios, N.; Novell-Leruth, G.; Whiting, P.; Liz-Marzán, L. M.; López, N. Theoretical description of the role of halides, silver, and surfactants on the structure of gold nanorods. *Nano Lett.* **2014**, *14*, 871−875.
(27) Meena, S. K.; Celiksoy, S.; Schäfer, P.; Henkel, A.; Sönnichsen, C.; Sulpizi, M. The role of halide ions in the anisotropic growth of gold nanoparticles: a microscopic, atomistic perspective. *Phys. Chem. Chem. Phys.* **2016**, *18*, 13246−13254.
(28) Liu, S.-H.; Balankura, T.; Fichthorn, K. A. Self-assembled monolayer structures of hexadecylamine on Cu surfaces: density-functional theory. *Phys. Chem. Chem. Phys.* **2016**, *18*, 32753−32761.
(29) Liu, S.-H.; Fichthorn, K. A. Interaction of alkylamines with Cu surfaces: a metal−organic many-body force field. *J. Phys. Chem. C* **2017**, *121*, 22531−22541.
(30) Liz-Marzán, L. M.; Grzelczak, M. Growing anisotropic crystals at the nanoscale. *Science* **2017**, *356*, 1120−1121.
(31) Vivek, J. P.; Burgess, I. J. Quaternary ammonium bromide surfactant adsorption on low-index surfaces of gold. 2. Au(100) and the role of crystallographic-dependent adsorption in the formation of anisotropic nanoparticles. *Langmuir* **2012**, *28*, 5040−5047.
(32) Kim, M. J.; Flowers, P. F.; Stewart, I. E.; Ye, S.; Baek, S.; Kim, J. J.; Wiley, B. J. Ethylenediamine promotes Cu nanowire growth by inhibiting oxidation of Cu(111). *J. Am. Chem. Soc.* **2017**, *139*, 277−284.
(33) Kim, M. J.; Alvarez, S.; Yan, T.; Tadepalli, V.; Fichthorn, K. A.; Wiley, B. J. Modulating the growth rate, aspect ratio, and yield of copper nanowires with alkylamines. *Chem. Mater.* **2018**, *30*, 2809−2818.
(34) Kresse, G.; Hafner, J. *Ab initio* molecular dynamics for liquid metals. *Phys. Rev. B: Condens. Matter Mater. Phys.* **1993**, *47*, 558−561.
(35) Kresse, G.; Hafner, J. *Ab initio* molecular-dynamics simulation of the liquid-metal−amorphous-semiconductor transition in germanium. *Phys. Rev. B: Condens. Matter Mater. Phys.* **1994**, *49*, 14251−14269.
(36) Kresse, G.; Furthmüller, J. Efficient iterative schemes for *ab initio* total-energy calculations using a plane-wave basis set. *Phys. Rev. B: Condens. Matter Mater. Phys.* **1996**, *54*, 11169−11186.
(37) Qi, X.; Fichthorn, K. A. Theory of the thermodynamic influence of solution-phase additives in shape-controlled nanocrystal synthesis. *Nanoscale* **2017**, *9*, 15635−15642.

DOI: 10.1021/jacs.8b08053
J. Am. Chem. Soc. 2018, 140, 14740−14746